Research Report

2005-02

Analysis of Optimal Stator Concentric Winding Patterns Design

W. Ouyang, T. A. Lipo, *A. EL-Antably

Department of Electrical and Computer Engineering
University of Wisconsin-Madison
1415 Engineering Drive
Madison, WI 53706

*Allison Transmission
Division of General Motors
P.O.Box 502650
Indianapolis, Indiana 46250

Work performed at WEMPEC sponsored by CPES.

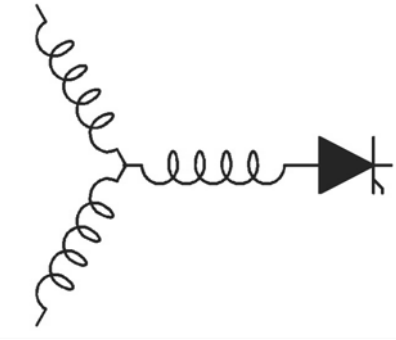

Wisconsin
Electric
Machines &
Power
Electronics
Consortium

University of Wisconsin-Madison
College of Engineering
Wisconsin Power Electronics Research Center
2559D Engineering Hall
1415 Engineering Drive
Madison WI 53706-1691

Analysis of Optimal Stator Concentric Winding Patterns Design

Wen Ouyang T.A. Lipo
Department of Electrical and Computer Engineering
University of Wisconsin-Madison
1415 Engineering Drive
Madison, WI 53706

Ahmed. EL-Antably
Allison Transmission
Division of General Motors
P.O.Box 502650
Indianapolis, Indiana 46250

***Abstract* — Most small induction motors in current use employ concentric windings which have equal numbers of turns per coil. An optimal choice of turns can achieve better distribution of MMF in the gap while keeping the turns in each slot essentially the same. In this paper, the air gap Magnetic Motive Force (MMF) harmonics of electrical machine created by the stator concentric windings with sinusoidal current injection are investigated. The air gap MMF is modeled ideally by a linear winding function, which simplifies the MMF expression significantly by neglecting the slot effects and saturation for uniform air-gap machines. By evaluating the harmonic property of the synthesized three phase air gap MMF waveform, optimal winding patterns can be developed for conventional choices of phase belts.**

***Keywords* — Concentric Windings, MMF, Harmonics, Induction Motor Windings**

I. INTRODUCTION

Concentric windings are widely used in electrical machines using random wound coils. Random wound coils are more amenable for factory automation compared with the copper bars used for higher power rating machines. They can be nested in a manner such that the entire phase group windings can be inserted into slots in one operation, while the overlapping nature of the more traditional lap winding makes them difficult to insert.

In the concentric winding coil fabrication, the coils for one phase belt are usually wound in a very simple manner, i.e., with equal turns for each coil. However, the automation process nowadays makes it quite easy for the coils to be wound more flexibly without much cost increase. In this paper, the optimal concentric winding patterns for various phase belts and slot number/pole/phase are investigated based on the winding function principle. Although the slot shape and stator saturation effect also contribute significantly to the air gap flux distribution, the general expression based on the winding ampere-turns for the air gap MMF distribution is the conventional means for distinguishing the harmonics due to winding layout from those due to saturation and by slot permeance variations.

II. WINDING FUNCTION

In order to analyze the air gap field distribution by the stator exciting current for the uniform air-gap machine, a linear model based on ampere-turns is illustrated in Figure 1. The assumptions are made here for the problem simplification:

1) $\mu = \infty$ for the iron sections

2) $\mu = \mu_0$ for the uniform air gap

3) Saturation and slot effects are neglected

4) Air gap flux is distributed uniformly between slots

5) Balanced sinusoidal current injection and symmetric winding layout for the periodic flux distribution in the air gap.

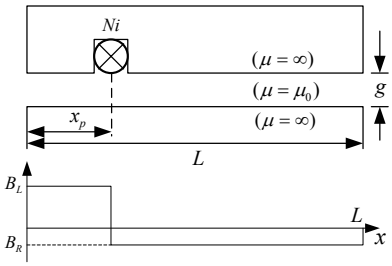

Fig.1: Air gap flux model

As shown in Fig. 1, the distribution of air gap magnetic motive force (MMF) determines the air gap flux shape directly in this model. The basic relation equations between MMF and flux density are provided in (1):

$$MMF = N \cdot i = R_L \cdot B_L \cdot x_p \cdot d + R_R \cdot B_R \cdot (L - x_p) \cdot d \qquad (1)$$

where:

$N \cdot i$: product of winding turns and current.

R_L and R_R: reluctances for the air gap sections at left and right side of the slot.

B_L and B_R: uniformly distributed flux for the air gap sections at left and right side of the slot.

d: depth of the model (directed normally into the paper).

With the reference set to the slot position, noting the flux is balanced at left and right side of the slot for continuity (Gauss' Law), the flux densities for B_L and B_R can be obtained:

$$B_L = \mu_0 \frac{Ni}{g} \times \frac{L - x_p}{L} \quad (2)$$

$$B_R = -\mu_0 \frac{Ni}{g} \times \frac{x_p}{L} \quad (3)$$

By applying superposition principle, the air gap flux distribution for an arbitrary winding position can be easily obtained as illustrated in Figure 2.

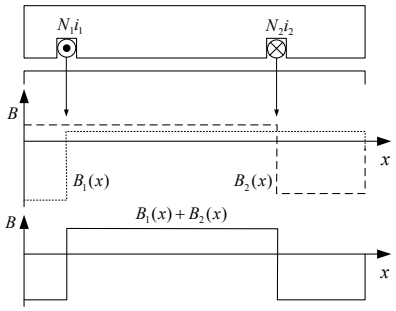

Fig.2: Air gap flux by superposition

Thus, the air gap flux for the concentric winding can be conveniently defined. An example is provided in Figure 3.

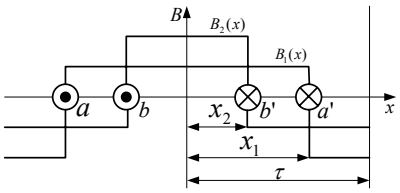

Fig.3: Air gap flux for a typical concentric winding

The Fourier series for the $B_1(x)$ can be expressed as (4) utilizing the even function property.

$$B_1(x) = a_0 + \sum_{n=1}^{\infty} a_n \cos\frac{n\pi}{\tau} x \quad (4)$$

where:

$$a_0 = \frac{1}{\tau}\int_0^{\tau} B_1(x)\,dx = 0 \quad (5)$$

$$a_n = \frac{2}{\tau}\int_0^{\tau} B_1(x)\cos\frac{n\pi}{\tau} x\,dx = \frac{2\mu_0 N_1 i_1(t)}{n\pi g}\sin\frac{n\pi}{\tau} x_1 \quad (6)$$

Note that (2) and (3) are used in the calculation of (6).

Thus, the air gap flux generated by one winding coil can be expressed as (7) which combine the space position and assumed sinusoidal current injection angle θ.

$$B(x,\theta) = \sum_{n=1}^{\infty} \left(\frac{2\mu_0 N\, i(\theta)}{n\pi g}\sin\frac{n\pi}{\tau} x\right)\cos\frac{n\pi}{\tau} x \quad (7)$$

The actual air gap flux can then be synthesized from all of the stator winding coils by superposition. With different turn numbers N_j in each slot and q coils for each pole, the full expression in closed form for the three phase air-gap flux can be derived as (8).

$$B(x,\theta) = \sum_{j=1}^{q}\sum_{n=1}^{\infty}\left(\frac{3\mu_0 N_j I}{n\pi g}\sin\frac{n\pi}{\tau} x_j\right)\left[\cos\left(\theta - \frac{(3n-2)\pi}{\tau} x\right) + \cos\left(\theta + \frac{(3n-1)\pi}{\tau} x\right)\right] \quad (8)$$

Note that the x_j denotes the different coil spans, and I is the current amplitude.

By selecting the turns number of each coil of the concentric winding, the harmonic content in the resulting air gap MMF (flux) waveform can be minimized, which leads to the possibility of an optimal winding pattern.

III. Optimal Winding Patterns

To optimize the concentric winding patterns, the minimum THD is set as the objective function combined with the balance of coil turns in each slot (the total turns difference for each slot is limited to 1 or 2). Four typical cases with standard phase belts of 60, 90, 120, and 180 degree are briefly discussed in this paper.

60° phase belt

Table 1 describes the concentric winding layout under one pole span for 60 phase belt with q =3. The minus sign denotes the reversed current direction for the windings in a given slot. '0' means no corresponding phase windings are in that slot.

Slot #	**1**	**2**	**3**	**4**	**5**	**6**	**7**	**8**	**9**
Phase C	**0**	**0**	**0**	**0**	**0**	**0**	**c**	**c**	**c**
Phase B	**b**	**b**	**b**	**0**	**0**	**0**	**0**	**0**	**0**
Phase A	**0**	**0**	**0**	**-a**	**-a**	**-a**	**0**	**0**	**0**

Table.1: Winding layout for 60 degree phase belt, q = 3.

Optimal winding patterns for the 60 degree phase belt and q = 3 with different total coil turns per pole per phase are listed in Table 2. The winding fundamental coefficient Kw1 and winding THD (considering up to the 99th harmonic) are also provided. The optimal pattern for this case with only one layer of winding converges to an equal number of turns Ntotal for each slot.

Ntotal	N1	N2	N3	Kw1	THD
9	3	3	3	0.9598	0.1134
10	3	4	3	0.9638	0.1183
11	4	3	4	0.9561	0.1151
12	4	4	4	0.9598	0.1134
13	4	5	4	0.9629	0.1166
14	5	4	5	0.9569	0.1142
15	5	5	5	0.9598	0.1134
16	5	6	5	0.9623	0.1156
17	6	5	6	0.9574	0.1138
18	6	6	6	0.9598	0.1134
19	6	7	6	0.9619	0.1151
20	7	6	7	0.9578	0.1136
21	7	7	7	0.9598	0.1134
22	7	8	7	0.9616	0.1147
23	8	7	8	0.9581	0.1134
24	8	8	8	0.9598	0.1134
25	8	9	8	0.9614	0.1145
26	9	8	9	0.9583	0.1134
27	9	9	9	0.9598	0.1134
28	10	8	10	0.9569	0.1142
29	10	9	10	0.9584	0.1133
30	10	10	10	0.9598	0.1134

Table.2: Optimal winding patterns for 60 degree phase belt, $q = 3$.

Figure.4 illustrates the harmonic spectrum for the winding configuration of 60 phase belt, $q = 3$, with one turn coil per slot and with unit current injection. The harmonic with negative amplitude, such as 19^{th}, 35^{th}, rotates in the opposite direction compared with the fundamental. Since the layouts basically follow the patterns of equal turns in each slot, the fundamental winding coefficient and wind THD are maintained at values close to each other. Basically, the symmetric three phase winding and balance current injections can make the synthesized air-gap MMF sinusoidal naturally. With equal turns coil in each slot, the irregularity created by the unequal step height (unequal turns) is thus reduced to the minimum. The incidental harmonics with this winding configuration, such as 5^{th}, 7^{th}, 11^{th}, …, also reach their minimum values with an equal turns pattern.

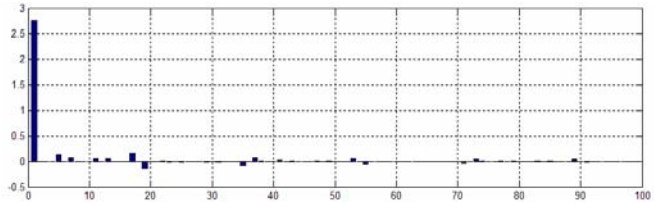

Figure 4: Typical harmonic spectrum for 60 phase belt, $q = 3$, a_1=2.75

For the higher order harmonics, it is interesting to note that the harmonics mainly concentrates around the multiples of the slot number covered by one pole pair. In this case, one pole pair spans 18 slots, resulting the attenuated harmonics of 17^{th}, 19^{th}, 35^{th}, 37^{th}, … . These characteristic slot harmonics will appear in the normal way at the order as described in equation (9) for three phase machines [1].

$$h_k = 6kq \pm 1 \qquad (9)$$

90^o phase belt

The typical concentric winding layout under one pole span for 90 phase belt and q =2 is described in Table.3. Note that the windings from different phases begin to share one slot.

Slot #	**1**	**2**	**3**	**4**	**5**	**6**
Phase C	**0**	**0**	**0**	**c**	**c**	**c**
Phase B	**b**	**b**	**0**	**0**	**0**	**-b**
Phase A	**0**	**-a**	**-a**	**-a**	**0**	**0**

Table.3: Winding configuration for 90 degree phase belt, $q = 2$.

The optimized winding patterns for 90^o phase belt with $q = 2$ are provided in Table 4. The pattern numbers in the slots are distributed in a symmetric manner due to the constraints of a balanced three phase winding configuration and balanced current injection, which is also coincident with the total turns number difference limit requirement.

Ntotal	N1	N2	N3	Kw1	THD
5	1	3	1	0.9464	0.1633
6	2	2	2	0.9107	0.1633
7	2	3	2	0.9234	0.1480
8	2	4	2	0.9330	0.1480
9	2	5	2	0.9405	0.1546
10	3	4	3	0.9196	0.1508
11	3	5	3	0.9269	0.1468
12	3	6	3	0.9330	0.1480
13	3	7	3	0.9382	0.1520
14	4	6	4	0.9234	0.1480
15	4	7	4	0.9286	0.1467
16	4	8	4	0.9330	0.1480
17	4	8	5	0.9291	0.1504
18	5	8	5	0.9256	0.1471
19	5	9	5	0.9295	0.1468
20	5	10	5	0.9330	0.1480
21	5	10	6	0.9298	0.1493
22	6	10	6	0.9269	0.1468
23	6	11	6	0.9301	0.1469
24	6	12	6	0.9330	0.1480
25	6	12	7	0.9303	0.1487
26	7	12	7	0.9279	0.1467
27	7	13	7	0.9305	0.1470
28	7	14	7	0.9330	0.1480
29	7	14	8	0.9307	0.1483
30	8	14	8	0.9286	0.1467

Table.4: Optimal winding patterns for 90 degree phase belt, $q = 2$.

For comparison, the spectrum of the winding patterns with equal turns in slots (10-10-10) and optimized pattern (8-14-8) are provided in Figure 5. One of the most significant contributions of the optimized winding pattern is the elimination of the harmonics of 5^{th} and 7^{th}, which benefits the machine efficiency, torque ripple, noise and vibrations, etc, although the total THD deduction looks small. Meanwhile, the winding coefficient is also increased from 0.9107 (same as 1-1-1) to 0.9286, which means a machine design with more effective material usage.

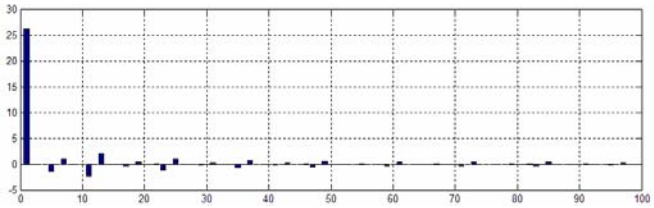

Figure 5.a: Harmonic spectrum for q=2, winding pattern: 10-10-10. THD=16.33%, a_1=26.09

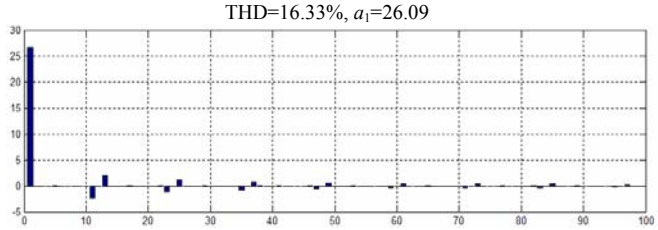

Figure 5.b: Harmonic spectrum for q=2, winding pattern: 8-14-8. THD=14.67%, a_1=26.6.

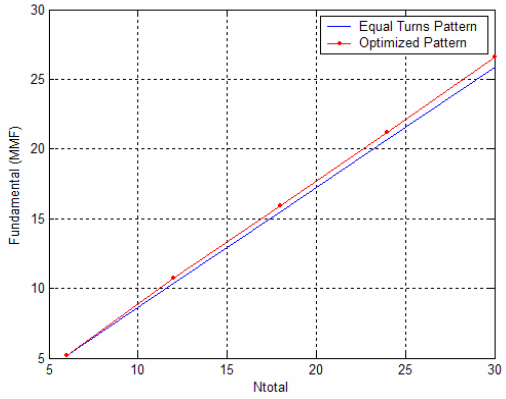

Figure.6: Fundamental amplitude comparison of equal turns pattern and optimized patterns for 90º phase belt, $q = 4$.

Moreover, the fundamental of the air gap MMF is enhanced by the optimal winding pattern as well. Figure.6 illustrates the fundamental enhancement by the optimized patterns for the 90º phase belt with $q = 4$. The benefit of fundamental enhancement of the optimal pattern is obviously exhibited with an increased winding turns number, which directly contributes to the torque production.

120º phase belt

The three phase winding configuration under one pole pitch for 120 degree phase belt with $q = 2$ is provided in Table 5.

Slot #	1	2	3	4	5	6
Phase C	-c	0	0	c	c	c
Phase B	b	b	b	0	0	-b
Phase A	0	-a	-a	-a	-a	0

Table.5: Winding configuration for 120 degree phase belt, $q = 2$.

The optimized winding patterns for this winding configuration are listed in Table 6. The symmetric property is still shared by those patterns. However, with an increased slot number under one pole pitch span, the fundamental coefficient of the winding has deteriorated due to the short pitch effect. It is also interesting to note that the THDs converge to almost the same value, which is actually the combined effect of the intrinsic harmonics as depicted by the plots after optimization.

Ntotal	N1	N2	N3	N4	Kw1	THD
4	1	1	1	1	0.8365	0.1633
5	1	2	1	1	0.8624	0.1743
6	1	2	2	1	0.8797	0.1480
7	1	2	3	1	0.8920	0.1582
8	1	3	3	1	0.9012	0.1468
9	1	3	4	1	0.9084	0.1540
10	1	4	4	1	0.9142	0.1480
11	1	4	5	1	0.9189	0.1531
12	2	4	4	2	0.8797	0.1480
13	2	4	5	2	0.8863	0.1506
14	2	5	5	2	0.8920	0.1468
15	2	5	6	2	0.8969	0.1493
16	2	6	6	2	0.9012	0.1468
17	2	6	7	2	0.9050	0.1490
18	2	7	7	2	0.9084	0.1473
19	3	6	7	3	0.8842	0.1490
20	3	7	7	3	0.8883	0.1470
21	3	8	7	3	0.8920	0.1481
22	3	8	8	3	0.8953	0.1467
23	3	8	9	3	0.8984	0.1478
24	3	9	9	3	0.9012	0.1468
25	3	9	10	3	0.9038	0.1479
26	3	10	10	3	0.9062	0.1471
27	4	9	10	4	0.8892	0.1478
28	4	10	10	4	0.8920	0.1468
29	4	10	11	4	0.8945	0.1474
30	4	11	11	4	0.8969	0.1467

Table.6: Optimal winding patterns for 120 degree phase belt, $q = 2$.

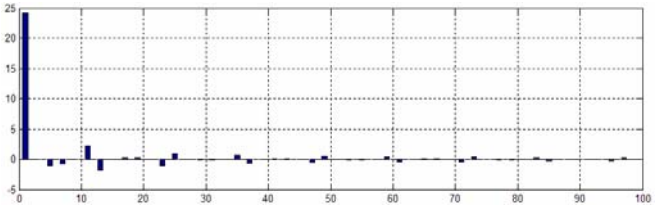

Figure 7.a: Harmonic spectrum for $q = 2$, winding pattern: 7-8-8-7.
THD=15.88%, a_1=24.21

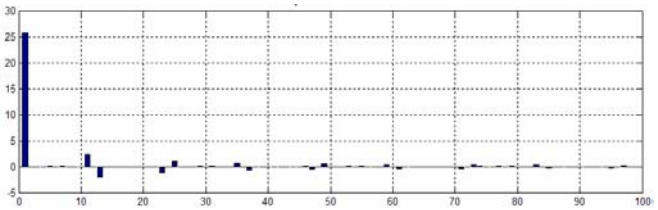

Figure 7.b: Harmonic spectrum for $q = 2$, winding pattern: 4-11-11-4.
THD=14.67%, a_1=25.69

Similarly, the 5th and 7th harmonics are eliminated by the optimal winding patterns. One can note also, that the fundamental component is strengthened.

180º phase belt

For completeness of the discussion, the optimal winding patterns for the 180 degree phase belt are also investigated. The three phase winding configuration under one pole pitch span is illustrated in Table 7.

Slot #	1	2	3	4	5	6
Phase C	-c	-c	c	c	c	c
Phase B	b	b	b	b	-b	-b
Phase A	-a	-a	-a	-a	-a	-a

Table.7: Winding configuration for 180 degree phase belt, $q = 2$.

The optimized patterns and the typical winding harmonics spectrum are provided in Table 8 and Figure 8.

Ntotal	N1	N2	N3	N4	N5	N6	Kw1	THD
4	0	1	1	1	1	0	0.8365	0.1585
5	0	1	1	2	0	1	0.7727	0.1585
6	0	1	2	2	1	0	0.8797	0.1430
7	0	2	1	2	1	1	0.7540	0.1430
8	0	1	3	3	1	0	0.9012	0.1418
9	0	2	2	3	1	1	0.8011	0.1418
10	1	2	2	2	2	1	0.7210	0.1418
11	1	3	1	2	2	2	0.6554	0.1418
12	2	3	1	1	3	2	0.6008	0.1419
13	2	4	0	1	3	3	0.5546	0.1419
14	0	2	5	5	2	0	0.8920	0.1418
15	0	3	4	5	2	1	0.8325	0.1418
16	1	3	4	4	3	1	0.7805	0.1418
17	1	4	3	4	3	2	0.7346	0.1418
18	1	3	5	5	3	1	0.8011	0.1418
19	2	3	5	4	4	1	0.7589	0.1418
20	2	4	4	4	4	2	0.7210	0.1418
21	2	5	3	4	4	3	0.6866	0.1418
22	0	3	8	8	3	0	0.8953	0.1417
23	0	4	7	8	3	1	0.8564	0.1417
24	1	4	7	7	4	1	0.8207	0.1417
25	1	5	6	7	4	2	0.7879	0.1417
26	2	5	6	6	5	2	0.7576	0.1417
27	2	6	5	6	5	3	0.7295	0.1417
28	3	6	5	5	6	3	0.7035	0.1417
29	3	7	4	5	6	4	0.6792	0.1417
30	4	7	4	4	7	4	0.6566	0.1418

Table.8: Optimal winding patterns for 180 degree phase belt, $q = 2$.

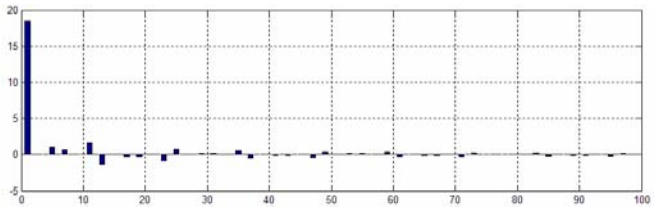

Figure 8.a: Harmonic spectrum for $q = 2$, winding pattern: 5-5-5-5-5-5.
THD=16.33%, a_1=18.448

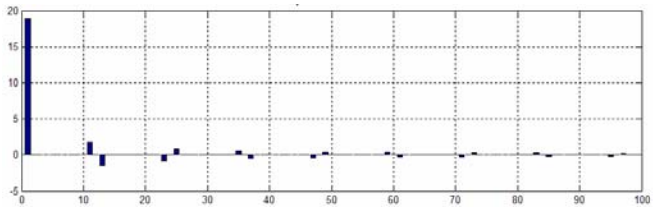

Figure 8.b: Harmonic spectrum for $\underline{q}$ = 2, winding pattern: 4-7-4-4-7-4. THD=14.67%, a_1=18.81

Basically, the optimal patterns for the 180 degree phase belt share similar properties as discussed before, while the winding fundamental coefficient further deteriorates. However the overall result can be integrated into the optimization objectives to obtain a higher fundamental coefficient for a given application.

IV. CONCLUSION

This paper investigates optimal winding patterns for the concentric three phase windings based on a traditional uniform air gap MMF harmonic analysis. The optimized patterns contribute to the reduction of THDs, especially the elimination of 5^{th} and 7^{th} MMF harmonics, which benefits the machine efficiency, noise and vibration. Meanwhile, the enhanced air gap MMF fundamental component favors torque production, and the higher winding coefficient makes the design of the machine materials more effective. The prevalence of automatic winding fabrication processes should make it possible to produce the concentric windings with different coil turns at negligible additional cost.

REFERENCE

[1] T.A.Lipo, "*Introduction to AC Machine Design*", University of Wisconsin, 2004.

[2] Sang-Baeck Yoon, "Optimization of Winding Turns for Concentric Windings with 180 and 120 degree phase belts", Report, University of Wisconsin, May, 1999.

[3] Hamid A. Toliyat, T.A. Lipo, J.C. White, "Analysis of a Concentrated Winding induction machine for Adjustable Speed Drive Applications", IEEE Transaction on Energy Conversion, Vol.6, No.4, Dec, 1991.